Research Article | Open Access

Microstructures

Kim *et al. Microstructures* **2026**, *6*, 2026051 **DOI:**10.20517/microstructures.2025.59

Development of nano-sized $LiFePO_4$ dry cathodes with enhanced flexibility and mechanical robustness for roll-to-roll dry coating process

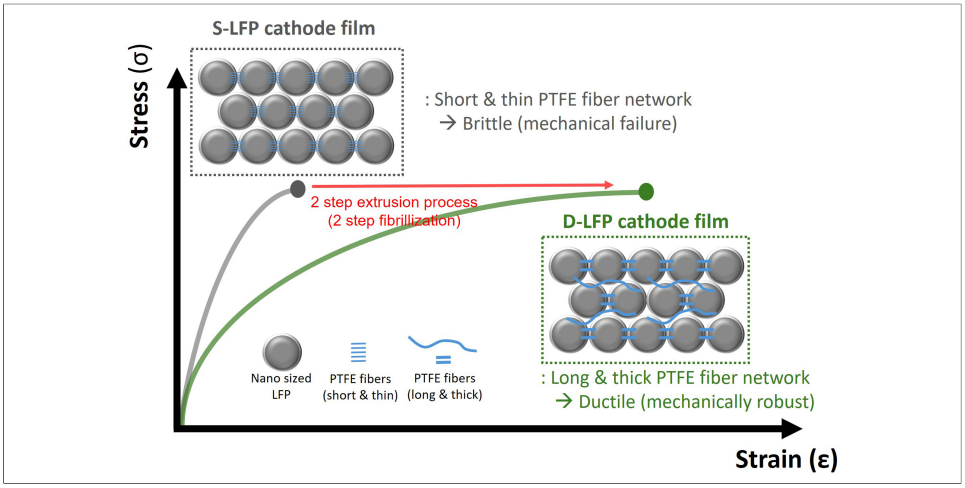
Jiwoon Kim[1,#], Minsung Kim[1,#], Seungmin Han[1], Ungyu Paik[1], Taeseup Song[1,2]

Keywords:
Li-ion batteries, thick electrode, roll-to-roll dry coating process, lithium iron phosphate, PTFE fibrillization

Citation: Kim, J.; Kim, M.; Han, S.; Paik, U.; Song, T. Development of nano-sized $LiFePO_4$ dry cathodes with enhanced flexibility and mechanical robustness for roll-to-roll dry coating process. *Microstructures* **2026**, *6*, 2026051. https://dx.doi.org/10.20517/microstructures.2025.59

Received: 29 Apr 2025 **First Decision:** 23 May 2025 **Revised:** 6 Jun 2025 **Accepted:** 12 Jun 2025 **Published:** 29 Apr 2026

Academic Editor: Shaobo Cheng **Copy Editor:** Ping Zhang **Production Editor:** Ping Zhang



Abstract

The polytetrafluoroethylene (PTFE) binder-based roll-to-roll dry coating process has emerged as a promising alternative to conventional slurry-based methods for fabricating thick electrodes in high-energy-density lithium-ion batteries (LIBs). However, applying nano-sized lithium iron phosphate ($LiFePO_4$, LFP) to this process remains challenging, as the high specific surface area of nano-sized LFP leads to the formation of short and thin PTFE fiber network that cannot ensure the mechanical integrity of dry cathode at low PTFE binder content. Consequently, the nano-sized LFP dry cathode suffers from poor flexibility and mechanical brittleness, limiting its applicability in roll-to-roll processing. In this study, we investigated the fibrillization behavior of PTFE binders depending on the particle size of LFP, to elucidate the origin of mechanical degradation in nano-sized LFP dry cathodes. Our results revealed that nano-sized LFP facilitates excessive PTFE fibrillization, generating fragile and weak networks with short and long PTFE fibers, leading to the mechanical degradation of nano-sized LFP dry cathodes. To address this issue, we introduced a two-step extrusion process that promotes the formation of thick and long PTFE fiber

[1]Department of Energy Engineering, Hanyang University, Seoul 04673, Republic of Korea.
[2]Department of Battery Engineering, Hanyang University, Seoul 04673, Republic of Korea.
[#]Authors contributed equally.

Correspondence to: Prof. Ungyu Paik, Department of Energy Engineering, Hanyang University, Wangsimni-ro Seongdong-gu, Seoul 04673, Republic of Korea. E-mail: upaik@hanyang.ac.kr; Prof. Taeseup Song, Department of Energy Engineering, Hanyang University, Wangsimni-ro Seongdong-gu, Seoul 04673, Republic of Korea; Department of Battery Engineering, Hanyang University, Wangsimni-ro Seongdong-gu Seoul 04673, Republic of Korea. E-mail: tssong@hanyang.ac.kr

networks within nano-sized LFP dry cathodes. This strategy enabled the fabrication of flexible and mechanically robust nano-sized LFP cathode film with only 2 wt% PTFE binder. The developed LFP dry cathodes exhibited excellent compatibility with thick electrode designs and achieved high areal capacities (7 mAh cm^{-2}, 2.7 g/cc), offering a scalable solution for next-generation LFP-based LIBs.

INTRODUCTION

The rapid growth of the electric vehicle (EV) market has accelerated the demand for high-energy-density lithium-ion batteries (LIBs) that are both safe and cost-competitive[1,2]. While high nickel layered oxide cathodes [e.g., lithium nickel cobalt manganese oxide (NCM), lithium nickel cobalt aluminum oxide (NCA)] have been widely adopted due to their higher capacity over 200 mAh g^{-1}, they face issues such as unstable raw material prices, poor thermal safety, and growing concerns about both safety and production cost[3,4]. In this context, lithium iron phosphate ($LiFePO_4$, LFP) cathodes are attracting significant attention for applications where safety, lifespan, and cost-effectiveness are critical-such as in mid-range EVs and stationary energy storage systems (ESS)[5]. LFP offers notable advantages including high thermal and chemical stability, long cycle life, and low cost[6-9]. However, its relatively low theoretical capacity (170 mAh g^{-1}), limited operating voltage (3.2~3.4 V), and intrinsically poor electronic and ionic conductivity limit its suitability for applications requiring high volumetric and gravimetric energy density, such as EV industry[10]. To address these limitations, research has focused on thick electrode designs that increase the areal loading of active material, thereby improving the energy density of LIBs at the cell level[11-13].

However, the fabrication of thick electrodes is difficult using conventional slurry-based (wet coating) methods. The wet coating processes suffer from issues such as binder migration during solvent evaporation, leading to inhomogeneous pore distribution and reduced adhesion between electrode and current collectors, thereby leading to the deterioration in electrochemical performance-particularly when electrode thickness increases[14]. Accordingly, the polytetrafluoroethylene (PTFE)-based roll-to-roll dry coating processes have emerged as a promising alternative to overcome the limitations of wet coating processes[15-18]. In the roll-to-roll dry coating process, active materials, conductive additives, and polymeric binders are mechanically dry-mixed under high shear forces to form dry mixtures. These dry mixtures are then calendered and laminated to form free-standing electrode film and dry electrode without requiring any solvent, drying, or solvent recovery steps [Supplementary Figure 1]. A critical advantage of the dry coating process lies in the fibrillization behavior of PTFE binders, which forms fibrous networks under mechanical shear stress[19-22]. These PTFE fiber networks improve the adhesion among active material particles, thereby enhancing the mechanical integrity and structural stability of the electrode. As a result, research on LFP dry electrodes using dry coating processes has gained considerable attention in recent years[23,24].

However, the application of dry coating processes to LFP still presents several technical challenges. Given the low Li-ion and electronic conductivity of LFP, the nano-sized particles with their high specific surface area (SSA) are essential to improve Li-ion and electron transport pathways within the electrode[25-27]. Yet, the high SSA of nano-sized LFP requires a higher binder content to ensure sufficient mechanical cohesion between LFP particles. In contrast, higher binder content lowers the proportion of LFP particles, lowering the overall energy density and thereby reducing the effectiveness of thick electrode designs. Even more critically, nano-sized LFP dry cathodes with low PTFE binder content exhibit significant brittleness, making them susceptible to cracking and fracture. Unlike micro-sized NCA dry cathode and graphite dry anode films, nano-sized LFP dry cathode films showed poor mechanical properties with poor ductility and a high tendency for fracture of cathode film after bending, which severely limits their suitability for roll-to-roll processing [Supplementary Figures 2-4]. To address this issue, various conductive agents were tested to identify the most suitable one for the fabrication of nano-sized LFP dry cathodes. Moreover, the fibrillization

behavior of PTFE has been controlled by adjusting the screw configuration inside the extrusion equipment to develop the nano-sized LFP dry cathodes[28,29]. However, the underlying mechanism of this brittleness, as well as its correlation with characteristics of LFPs and PTFE fibrillization behavior, has yet to be fully elucidated. Accordingly, the application of the dry coating process to nano-sized LFP for thick cathode remains highly challenging.

In this study, we investigated the fibrillization behavior of PTFE depending on the particle size of carbon-coated LFP, revealing that nano-sized LFP leads to the formation of thin and short PTFE fiber network, resulting in brittle and mechanically poor dry cathode films. To address this issue, we proposed a simple but effective two-step extrusion process to promote the formation of thick and long PTFE fiber networks within nano-sized LFP dry cathodes. In the 1st stage, a dry mixture of LFP, carbon nanotube (CNT), and PTFE were extruded and ground to produce 1st granules. Then, these 1st granules were subjected to a second extrusion with additional PTFE and CNT (2nd stage). During the second extrusion, the 1st granules acted as pseudo-large particles, facilitating the formation of thick and long PTFE fibers within nano-sized LFP dry cathode film. This thick and long PTFE fiber network improved the binding properties and thereby enhanced the flexibility and mechanical robustness of the nano-sized LFP dry cathode film. Using this approach, we successfully fabricated nano-sized LFP dry cathodes containing only 2 wt% PTFE binder, achieving both enhanced mechanical flexibility and microstructural stability. The improved mechanical integrity enabled the fabrication of thick LFP electrodes with high areal capacities, demonstrating their suitability for high-energy-density lithium-ion batteries. These results provide new insights into the mechanical failure mechanisms of nano-LFP dry electrodes and offer a scalable process engineering strategy for the development of next-generation, high-performance LFP-based LIBs.

MATERIALS AND METHODS

Fabrication of LFP dry cathode film and dry cathode

LFP dry cathode films and dry cathodes were fabricated via a roll-to-roll dry coating process using $LiFePO_4$, PTFE binder, and either carbon black (CB) or carbon nanotube (CNT) as the conductive agents, supplied by Samsung SDI. The dry powder mixture was homogenized using a dry mixer (L8-2k, KMTECH, Korea). All dry mixing processes in this work were conducted at 6,000 RPM for 1 h. For the two-step extrusion process, the 1st stage was performed under the same conditions (6,000 RPM for 1 h), while the 2nd stage was conducted at 10,000 RPM for 3 min. The total amount of the composite (LFP/CNT/PTFE) used in each batch was 500 g. Then, the dry mixed powder was extruded using a twin-screw extruder (HCK 25-24/CPC, HANKOOK E.M, Korea), crushed into granules (L8-2k, KMTECH, Korea), and rolled into films using a roller (KRM-80, KMTECH, Korea). The final LFP dry cathode films were laminated onto carbon-coated aluminum (Al) current collectors using a roll press (mp200, Rohtech, Korea).

Materials characterization

The morphology and microstructure of the electrodes were observed using field-emission scanning electron microscopy (FE-SEM, JSM-7600F, JEOL, Japan). Particle size distribution of the LFP powders was measured using a laser diffraction analyzer (Mastersizer 3000, Malvern Instruments, UK), and their SSA was determined by Brunauer-Emmett-Teller (BET) analysis (3Flex, Micromeritics Instrument Corporation, UK). Thermal behavior and crystallinity of PTFE in the composites were analyzed by differential scanning calorimetry (DSC, Q20, TA Instruments, USA) under a nitrogen atmosphere. The surface properties of the carbon coating layer on LFP particles were investigated using Raman spectroscopy (LabRAM HR Evolution, HORIBA, Japan). Mechanical properties of the dry LFP cathode films were evaluated using a universal testing machine (UTM, AGS-J, Shimadzu, Japan) under a constant strain rate and a micro-indentation test using a Vickers indenter (STeP500 MCT3, Anton Paar) under a fixed load of 3 N. Bending test was performed by bending the dry LFP cathode film around a stainless steel rod to evaluate its flexibility.

Electronic conductivity (sheet resistance) was measured using a four-point probe system (MCP-T610, Mitsubishi, Japan).

Electrochemical evaluation

Electrochemical performance of the dry LFP cathodes was evaluated using 2032-type coin half cells assembled with Li metal (200 μm) as the counter electrode, a polypropylene (PP) separator (20 μm, Celgard 2400), and an electrolyte consisting of 1.15 M $LiPF_6$ in EC/EMC/DMC (3:5:2 by volume) with 5 wt% fluoroethylene carbonate (FEC, PANAX StarLyte, Korea). The active material loading of the cathodes was 7 mAh cm^{-2}, with a composite electrode density of 2.7 g/cc. Galvanostatic charge/discharge tests were conducted in the 2.5-3.9 V voltage range *vs.* Li/Li^+ using a battery cycler (TOSCAT-3000, Toyo System, Japan) to assess rate capability and cycling performance. Electrochemical impedance spectroscopy (EIS) was performed using a potentiostat/galvanostat (AUT85698, Metrohm, Switzerland) over a frequency range of 0.001-1,000,000 Hz.

RESULTS AND DISCUSSIONS

PTFE fibrillization behavior depending on the particle size of LFP

Two types of LFP - small-sized LFP (S-LFP, nano-sized LFP) and large-sized LFP (L-LFP) - were applied to the roll-to-roll dry coating process to investigate the effect of LFP particle size on PTFE fibrillization behavior. Particle size distribution analysis revealed that the S-LFP sample exhibits an average size near 700~800 nm, whereas L-LFP shows a broader distribution centered around 10 μm, as further confirmed by SEM images [Figure 1A and Supplementary Figure 5]. The BET measurement showed that S-LFP (20.62 $m^2 g^{-1}$) has a substantially higher SSA than L-LFP (5.34 $m^2 g^{-1}$), which is attributed to the smaller particle size of S-LFP [Figure 1B]. Then, to evaluate the effect of particle size on PTFE fibrillization behavior, LFP/PTFE granules with a weight ratio of 7:3 were prepared via dry mixing and extrusion processes. A high PTFE content with 30 wt% was intentionally used to clearly observe the difference in PTFE fibrillization behavior within LFP/PTFE granules depending on the particle size of LFPs. SEM analysis revealed a significant difference in PTFE fiber morphology depending on the particle size of LFP. In the S-LFP/PTFE granule, a thin PTFE fiber network was formed across the S-LFP particles, whereas the L-LFP/PTFE granule exhibited a network with thick PTFE fibers [Figure 1C]. The observed difference in morphology of PTFE fiber networks would be primarily attributed to variations in the SSA of LFP. During the extrusion-based dry coating process, PTFE undergoes fibrillization through deformation induced by frictional forces generated during interaction with LFP particles by mechanical shear force. As the particle size of LFP decreases, the increased SSA of LFP leads to a greater interfacial contact area between PTFE and LFP, which enhances the frictional forces and, consequently, the shear force transmitted to the PTFE, thereby promoting more excessive PTFE fibrillization. Based on this interpretation, it is inferred that the high SSA of S-LFP increases interfacial contact with PTFE, resulting in higher friction and shear forces to PTFE, which in turn accelerates PTFE fibrillization and leads to the formation of a thin PTFE fiber network within the LFP/PTFE granule. To confirm the degree of PTFE fibrillization within LFP/PTFE granules, DSC measurements were conducted [Figure 1D]. The melting enthalpy (ΔH_m) of PTFE in the LFP/PTFE granules was obtained by integrating the endothermic peak area of PTFE, and crystallinity of PTFE was calculated using the equation: crystallinity (%) = $\Delta H_m/\Delta H_{m,100\%}$, where $\Delta H_{m,100\%}$ is the enthalpy of 100% crystalline PTFE (82 J g^{-1})[30-32]. Because the crystalline regions of PTFE decreased by the mechanical shear force-induced deformation, a lower crystallinity of PTFE represents a higher degree of mechanical deformation and thus more excessive PTFE fibrillization[33]. The DSC results showed that the S-LFP/PTFE granule had a lower ΔH_m of 26.5 J g^{-1} compared to 32.3 J g^{-1} in the L-LFP/PTFE granule, corresponding to crystallinity values of 32.3% and 42.6%, respectively [Figure 1E]. These results confirm that PTFE fibrillization was more facilitated within the S-LFP/PTFE granule, consistent with the SEM observations.

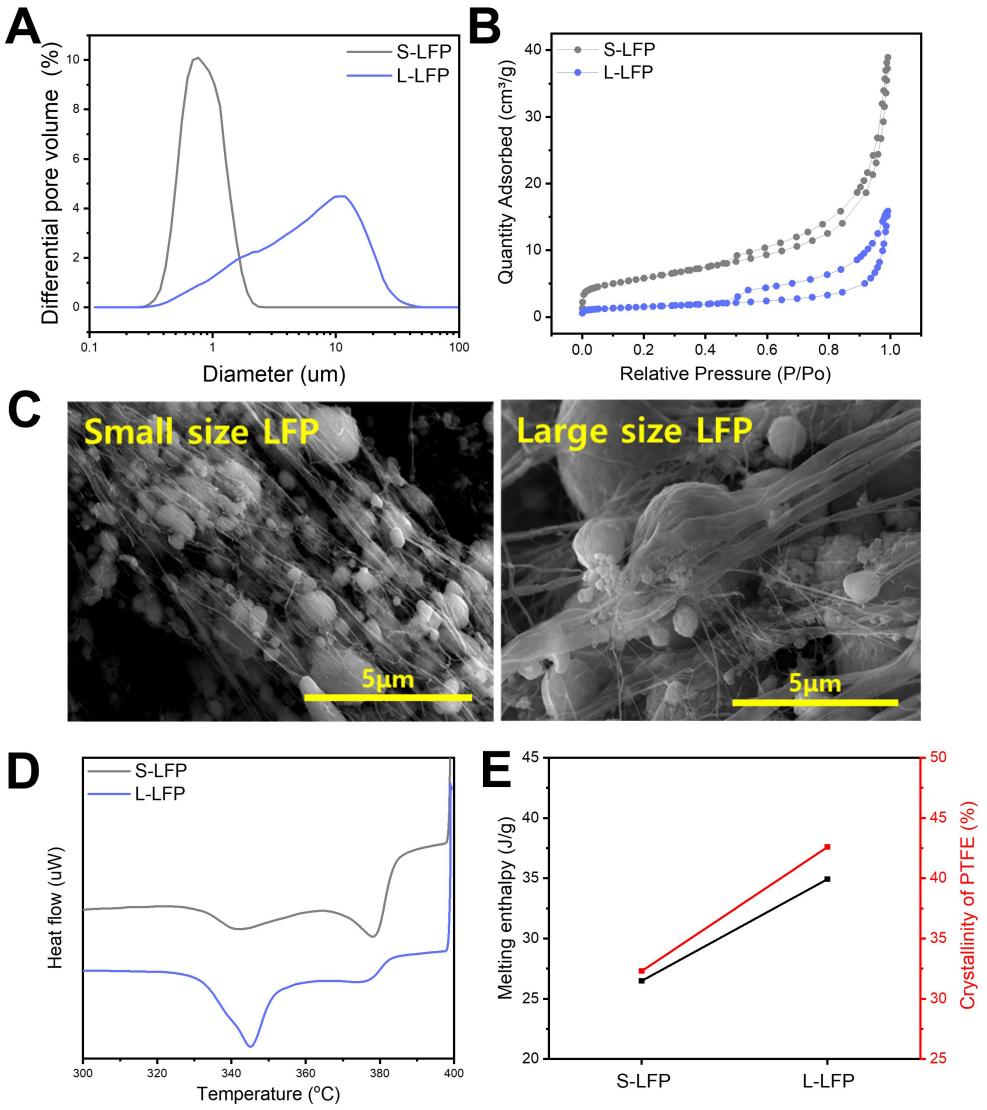


Figure 1. PTFE fibrillization behavior depending on the particle size of LFP. (A) Particle size distribution and (B) specific surface area of S-LFP and L-LFP; (C) SEM images of LFP/PTFE (7/3) granules after the extrusion process; (D) DSC measurement of LFP/PTFE (7/3) composite and (E) melting enthalpy and crystallinity of PTFE within LFP/PTFE (7/3) granules. PTFE: Polytetrafluoroethylene; LFP: $LiFePO_4$; S-LFP: small-sized LFP; L-LFP: large-sized LFP; SEM: scanning electron microscopy; DSC: differential scanning calorimetry.

Additionally, to examine whether the surface characteristics of the carbon layer coated on LFP could affect interfacial friction between LFP and PTFE and, thus, PTFE fibrillization behavior, Raman spectroscopy was conducted [Supplementary Figure 6]. The Raman spectra of S-LFP and L-LFP showed no significant differences in D/G ratio or peak width, suggesting that the carbon layer coated on LFP does not significantly affect the PTFE fibrillization behavior within the LFP/PTFE granule[34]. These results highlighted the critical role of LFP particle size in determining PTFE fibrillization behavior. Specifically, a higher SSA resulting from the smaller particle size of S-LFP increases the interfacial contact with PTFE, which induces the enhanced shear-induced deformation of PTFE and leads to excessive PTFE fibrillization, ultimately forming a thin PTFE fiber network within the LFP/PTFE granule.

Mechanical properties and microstructure of LFP dry cathodes

Then, to investigate how PTFE fibrillization behavior affects the mechanical properties of LFP dry cathode films in practical composition, LFP dry cathode films, with a composition ratio of LFP/CB/PTFE = 94:3:3,

were fabricated via roll-to-roll dry coating process. As shown in the digital images, the L-LFP dry cathode film successfully formed a continuous and flexible free-standing film. In contrast, the S-LFP dry cathode film appeared highly brittle, with severe edge cracking during the calendering process [Supplementary Figure 7]. To identify the origin of these differences, top- and cross-sectional view SEM analysis was conducted. The morphology of PTFE fibers observed in the LFP dry cathode films closely mirrored the PTFE fibrillization behavior previously seen in the LFP/PTFE (7/3) granules. In the S-LFP dry cathode film, a dense PTFE fiber network was found between the nano-sized particles; however, these PTFE fibers were thin and short, as clearly seen in the top-view images [Figure 2A and B]. In contrast, the L-LFP dry cathode film exhibited a thick and long PTFE fiber network, interconnecting the micro-sized LFP particles [Figure 2C and D]. To investigate the effect of PTFE fiber morphology on the mechanical properties of LFP dry cathode films, UTM measurement was conducted [Figure 2E]. The L-LFP dry cathode film showed a slightly higher tensile strength (0.57 MPa) compared to the S-LFP film (0.45 MPa). More importantly, a significant difference in elongation at break was observed: the L-LFP dry cathode film showed 4.25%, in contrast to 0.75% for the S-LFP film. This substantial increase in ductility resulted in a toughness of 2.0×10^6 J m^{-3} for the L-LFP film, which is approximately 8 times greater than that of the S-LFP film (0.25×10^6 J m^{-3}) [Figure 2F]. This remarkable enhancement in toughness is primarily attributed to the enhanced ductility of the L-LFP dry cathode film, likely due to the formation of a thick and long PTFE fiber network. Accordingly, this PTFE fiber network provides effective mechanical bridging between L-LFP particles, enabling the dry cathode film to withstand higher strain before fracture and resulting in a flexible and mechanically robust LFP dry cathode film. In contrast, the poor mechanical integrity of the S-LFP dry cathode film is likely associated with the formation of a thin and short PTFE fiber network, which fails to provide sufficient adhesion across the nano-sized LFP particles. As previously discussed, the SSA of S-LFP increases interfacial contact with PTFE, promoting excessive PTFE fibrillization under mechanical shear. As a result, the generated PTFE fibers are too thin to establish a mechanically robust network. Additionally, it is speculated that the limited interparticle spacing, due to the nanoscale size of LFP, may restrict the mobility of PTFE during the extrusion process, further hindering the development of long and continuous fiber networks. Collectively, these factors contribute to the formation of a thin and short PTFE fiber network within the S-LFP cathode film, resulting in brittleness and poor mechanical robustness [Figure 2G].

Two-step extrusion process for fabrication of LFP dry cathode film

To improve the flexibility and mechanical robustness of nano-sized LFP dry cathode films, we introduced a two-step extrusion process to facilitate the formation of a thick and long PTFE fiber network within the nano-sized LFP matrix. This two-step process was specifically designed to overcome the limitations of conventional dry processing, in which all components-LFP, CNT, and PTFE-are mixed, extruded, ground, and calendered in a single sequence. The CNTs were employed as conductive agents, not only to enhance electronic conductivity but also to contribute to the formation of a fiber network within the electrode due to their one-dimensional (1D) morphology[35]. As shown in the schematic illustration, the developed two-step extrusion process is divided into two stages [Figure 3A]. In the 1st stage, LFP is dry mixed with half of the total amount of CNT and half of the total amount of PTFE, followed by extrusion and grinding to form the 1st granules. Within the 1st granules, short and thin PTFE fibers were formed between closely packed nano-sized LFP particles, providing particle-to-particle adhesion. Although these fibers were not sufficiently long to form a robust fiber network, their presence contributed to the retention of the structural integrity of the 1st granules during the subsequent processing steps. In the 2nd stage, the remaining half of the total CNT and PTFE were dry mixed with the 1st granules, followed by extrusion and grinding to produce the 2nd granules, which were then calendered to fabricate the free-standing LFP dry cathode film. A key advantage of this two-step approach is that the relatively large particle size and rigid structure of the 1st granules act similarly to micro-sized particles. As a result, the contact area between the PTFE and 1st granules is reduced, which lowers the shear stress applied to the PTFE during the second extrusion and calendaring and leads to

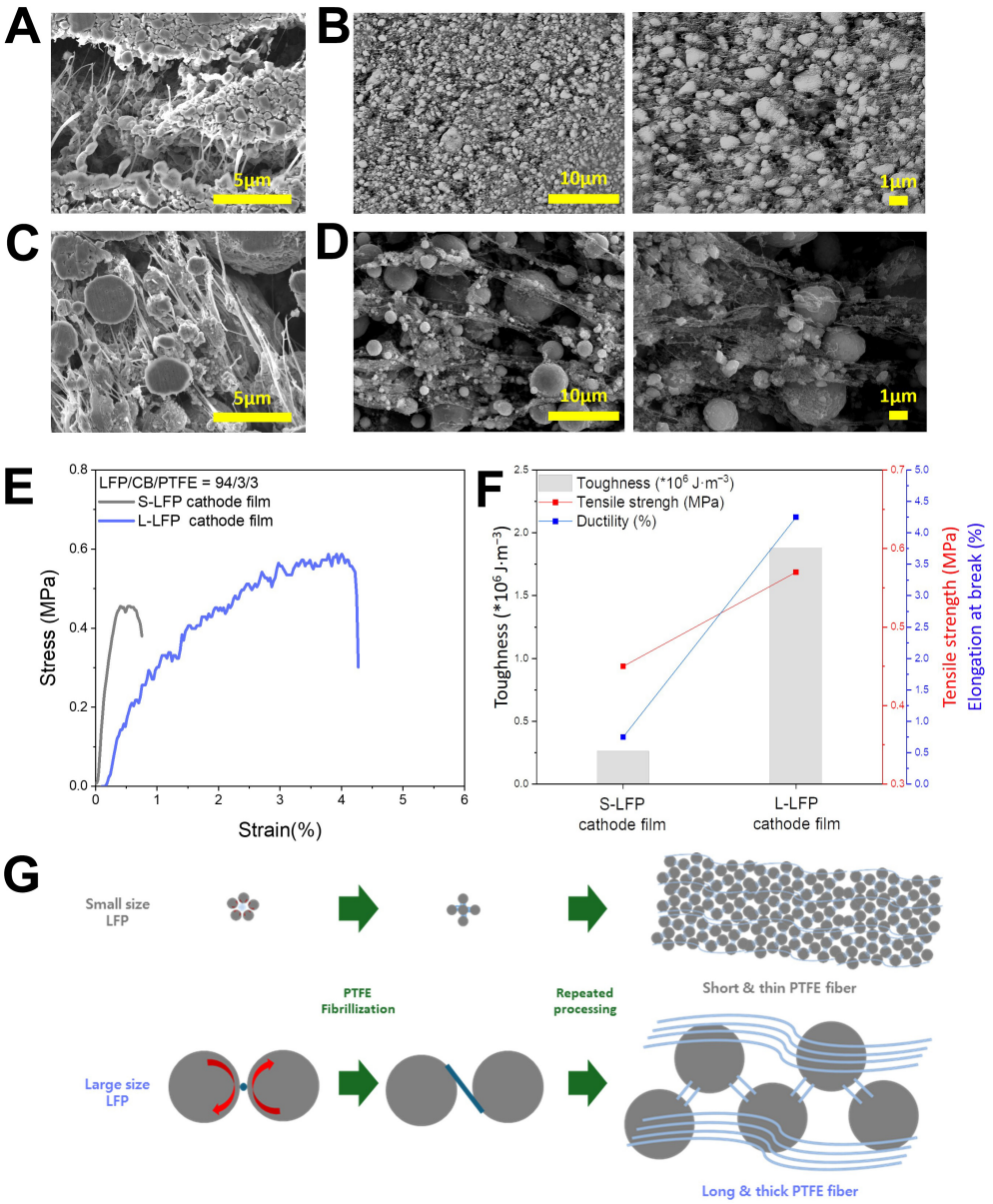


Figure 2. Mechanical properties and microstructure of dry LFP cathodes. SEM images of S-LFP cathode film, (A) cross-sectional view and (B) top view; SEM images of L-LFP cathode film; (C) cross-sectional view and (D) top view; (E) UTM measurement and (F) mechanical properties of dry LFP cathode films; (G) Schematic illustration of PTFE fiber network within dry LFP cathodes. LFP: $LiFePO_4$; S-LFP: small-sized LFP; L-LFP: large-sized LFP; SEM: scanning electron microscopy; UTM: universal testing machine.

the suppression of excessive PTFE fibrillization. Furthermore, the increased size of the 1st granules provides more free volume and intergranular space, improving the mobility of PTFE and allowing it to move more freely between the granules during processing. This enhanced mobility enables the formation of a thick and long PTFE fiber network, resulting in a flexible and mechanically robust nano-sized LFP dry cathode film. Then, we conducted SEM and particle size distribution analyses to gain further insight into the morphological evolution of the granules and dry cathode films after each stage, where the composition ratio of the LFP dry cathode film was LFP:CNT:PTFE of 94:3:3. The 1st granules exhibited a broad particle size distribution ranging from 1 μm to several hundred micrometers [Supplementary Figure 8]. SEM images of the 1st granules showed that short and thin PTFE fibers were located between the densely packed nano-sized LFP particles inside the granules [Figure 3B]. To observe the internal PTFE fiber network in the final dry cathode film, the nano-sized LFP dry cathode film fabricated via the two-step extrusion process-designated

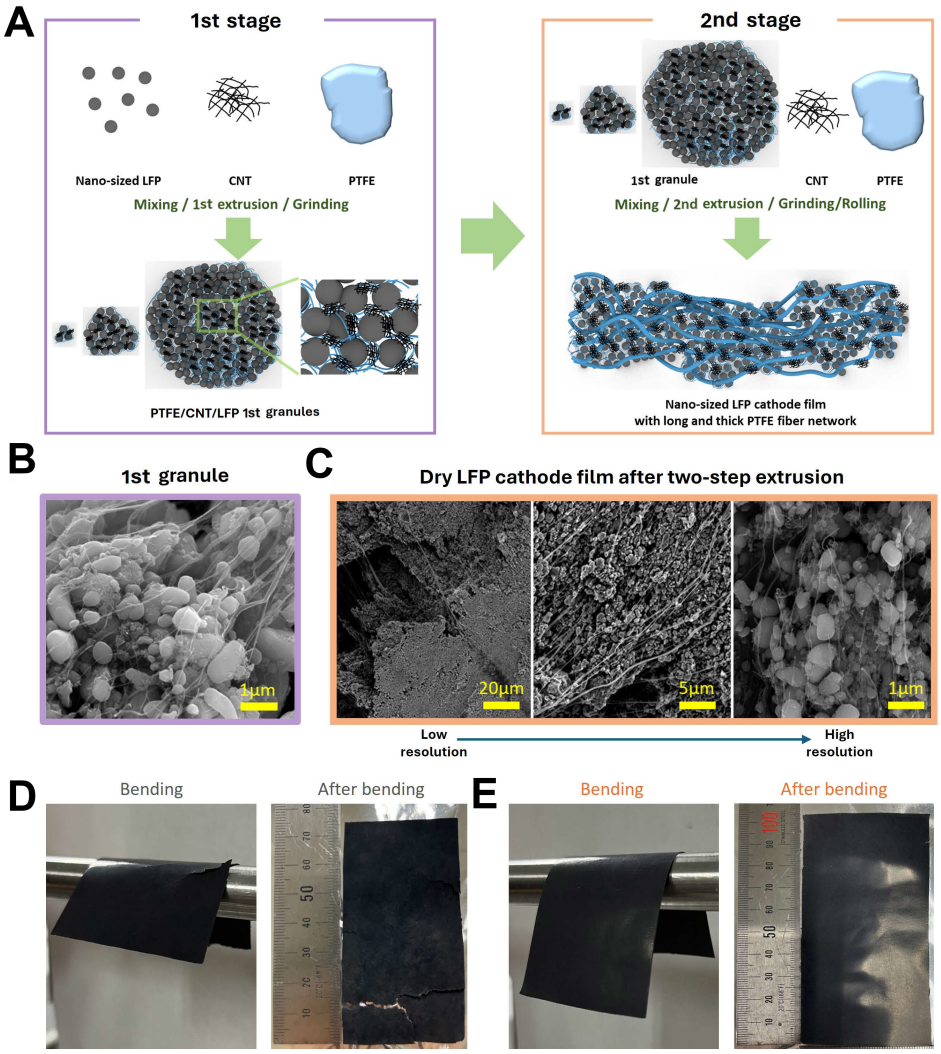


Figure 3. Two-step extrusion process for fabrication of dry LFP cathode film. (A) Schematic illustration of the two-step extrusion process for fabrication of dry LFP cathodes; left: 1st stage, right: 2nd stage; SEM images of (B) 1st granule after 1st stage and (C) cathode film after 2nd stage from low to high resolution; Digital images of (D) S-LFP cathode film and (E) D-LFP cathode film according to the bending test. LFP: $LiFePO_4$; SEM: scanning electron microscopy; S-LFP: small-sized LFP; D-LFP: developed LFP via two-step extrusion process.

as developed LFP (D-LFP)-was gently stretched to create a fractured surface, enabling clearer visualization of the internal PTFE fiber network morphology [Supplementary Figure 9]. Low-magnification SEM images of the fractured region revealed the formation of thick and long PTFE fiber networks bridging nano-sized LFP particles. High-magnification SEM images further revealed the coexistence of short and thin PTFE fibers that originated from the 1st granules. These results indicate that within the D-LFP dry cathode film, both short and thin PTFE fibers from the 1st stage and thick and long PTFE fibers from the 2nd stage are simultaneously present, forming a multi-scale fiber network [Figure 3C]. To evaluate the improvement in mechanical flexibility, we conducted bending tests comparing the D-LFP cathode film with a conventional S-LFP cathode film prepared with the same composition (LFP:CNT:PTFE = 94:3:3, by weight). Upon bending, the S-LFP film exhibited severe brittleness, with edge tearing and complete fracture, and failed to recover its original film structure [Figure 3D]. In contrast, the D-LFP film maintained its shape without visible cracking or damage during bending [Figure 3E]. This superior mechanical behavior is attributed to the well-developed PTFE fiber network formed through the two-step process, where the integration of thick and long PTFE fibers contributes to enhanced flexibility and mechanical robustness of the nano-sized LFP dry cathode film.

Mechanical properties and microstructure of LFP dry cathode films

To verify the enhancement of mechanical properties achieved via the two-step extrusion process, UTM and micro-indentation measurements were conducted on S-LFP and D-LFP dry cathode films with a composition ratio of LFP:CNT:PTFE = 94:3:3. The UTM results showed that the tensile strength of D-LFP was slightly higher (0.41 MPa) than that of S-LFP (0.39 MPa) [Figure 4A and Supplementary Figure 10]. In contrast, the difference in elongation at break was more pronounced: D-LFP exhibited a value of 2.9%, more than twice that of S-LFP, indicating a substantial improvement in ductility, attributed to the formation of a long and thick PTFE fiber network. As a result, the toughness of D-LFP achieved 0.75×10^6 J m^{-3}-more than double the value of S-LFP (0.30×10^6 J m^{-3})- indicating a significantly higher amount of mechanical energy required to reach fracture [Supplementary Figure 11][36,37]. Moreover, the micro-indentation results supported these findings. Under a constant load of 3 N, the indentation depth of D-LFP was 44 μm, compared to 51 μm for S-LFP, suggesting an increased resistance to deformation and enhanced mechanical robustness, associated with the robust PTFE fiber network formed during the 2nd stage [Figure 4B and Supplementary Figure 12]. Then, three types of LFP dry cathode films-S-LFP, D-LFP, and L-LFP-were fabricated with a composition of LFP:CNT:PTFE = 94:4:2 (by weight), to evaluate the mechanical properties under reduced binder content. The S-LFP dry cathode films were extremely brittle and exhibited poor film-forming capability, making it difficult to maintain a free-standing film structure. Although mechanical testing was still possible with great care, the films were fragile and challenging to handle. In contrast, both D-LFP and L-LFP dry cathode films successfully retained their free-standing film structure, indicating significantly improved mechanical integrity and film-forming capability under reduced binder conditions. Notably, the D-LFP dry cathode film exhibited significant flexibility in bending tests, showing no cracking or tearing and fully recovering its structure after bending [Supplementary Figure 13]. This improvement in mechanical properties was further supported by UTM results [Figure 4C and D, Supplementary Figure 14]. The D-LFP showed an elongation at break of 1.6%-more than three times that of S-LFP-and a toughness of 0.47×10^6 J m^{-3}, which is comparable to that of L-LFP (0.53×10^6 J m^{-3}). These findings highlight that the two-step extrusion process ensures sufficient film-forming capability under reduced binder content, without compromising mechanical robustness relative to conventional processes. Morphological analysis of LFP dry cathode films using top-view SEM further clarified the difference in electrode microstructure [Figure 4E]. In the S-LFP dry cathode films, PTFE fibers failed to bridge adjacent nano-sized LFP, resulting in the formation of cracks locally observed across the electrode, indicative of weak adhesion. This is attributed to the formation of a short and thin PTFE fiber network that is unevenly distributed throughout the electrode, resulting in regions with insufficient interparticle adhesion. In contrast to the S-LFP dry cathode films, the D-LFP and L-LFP dry cathode films exhibited no visible cracks, which can be attributed to the formation of long and thick PTFE fiber networks that effectively reinforce interparticle adhesion, thereby enhancing microstructural integrity. Consequently, the two-step extrusion process enables the fabrication of nano-LFP dry cathode films with enhanced flexibility and mechanical robustness, even under low binder content. This process-driven improvement reduces the need for higher PTFE content, enabling increased loading of conductive additives such as CNTs, which may further enhance electronic conductivity and electrochemical performance.

Electrochemical performance of LFP dry cathodes

The effect of improved mechanical integrity and microstructure on the electrical resistance and electrochemical performance of nano-LFP dry cathodes was investigated by fabricating three types of LFP dry cathodes-S-LFP, D-LFP, and L-LFP-with a fixed composition of LFP:CNT:PTFE = 94:4:2, an areal capacity of 7 mAh cm^{-2}, and an electrode density of 2.7 g cm^{-3}. The sheet resistance of LFP dry cathodes was measured using a four-point probe method [Figure 5A][38,39]. The S-LFP electrode exhibited a high sheet resistance of 11.97 Ω sq^{-1}, more than three times greater than those of the D-LFP and L-LFP electrodes. Additionally, S-LFP showed large standard variations in resistance values, likely due to localized cracks

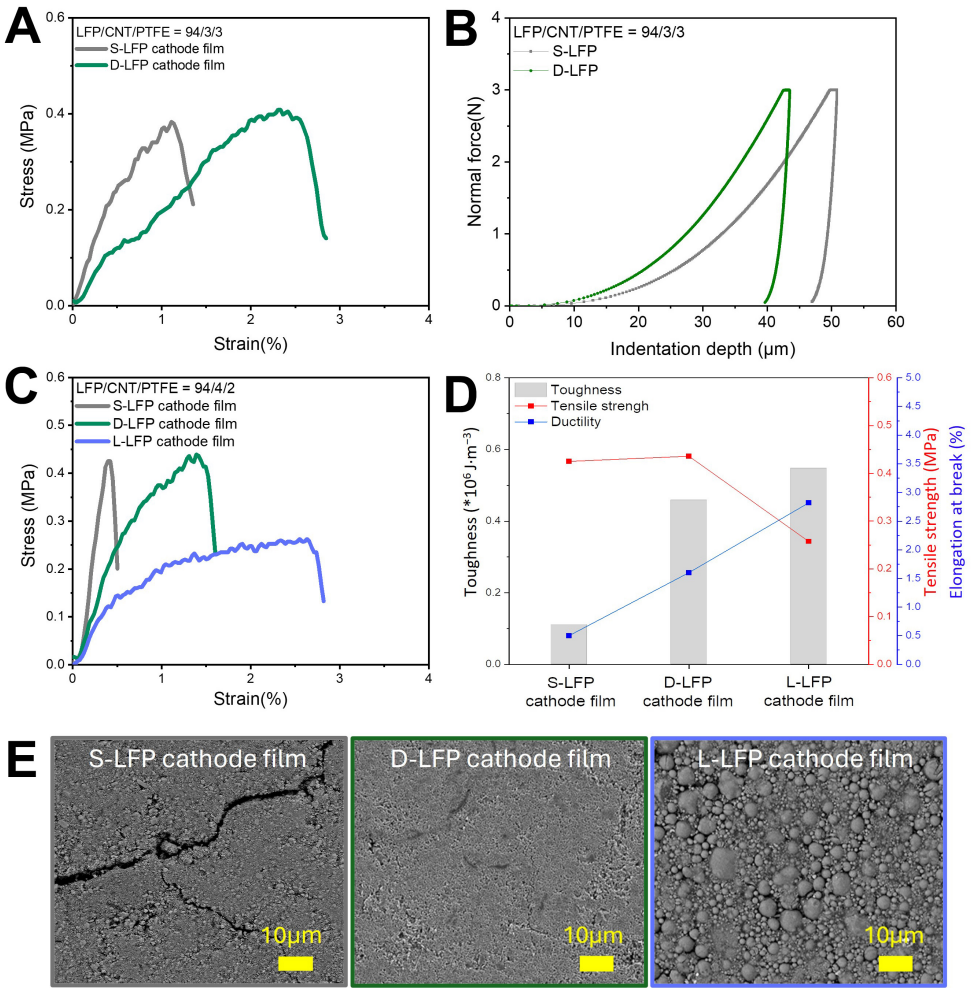


Figure 4. Mechanical properties and microstructure of dry LFP cathode films. (A) Stress-strain curve from UTM measurement and (B) micro-indentation test of dry LFP cathode films (LFP/CNT/PTFE = 94/3/3); (C) Stress-strain curve and (D) mechanical properties from UTM measurement; (E) Top view SEM images of dry LFP cathode films (LFP/CNT/PTFE = 94/4/2); left: S-LFP cathode film, middle: D-LFP Cathode film, right: L-LFP cathode film. LFP: $LiFePO_4$; UTM: universal testing machine; CNT: carbon nanotube; PTFE: polytetrafluoroethylene; SEM: scanning electron microscopy; S-LFP: small-sized LFP; L-LFP: large-sized LFP; D-LFP: developed LFP via two-step sxtrusion process.

observed in its top-view SEM images. In contrast, the D-LFP and L-LFP dry cathodes exhibited consistently low sheet resistance values with low standard variations, indicating that the well-formed, thick and long PTFE fiber networks ensured good interparticle adhesion and preserved continuous electronic pathways. These differences in electrical resistance were reflected in the rate capability test, evaluated using a half-cell configuration. During the formation condition (1st cycle at 0.1C-rate charge/discharge), no significant difference in initial capacity or coulombic efficiency was observed across the three LFP dry cathodes [Figure 5B]. However, as the discharge rate increased, the S-LFP dry cathode showed a steep degradation in discharge capacity, while D-LFP and L-LFP dry cathodes maintained a stable discharge capacity up to 0.5C rate. Beyond 1.0C rate, the L-LFP dry cathode began to exhibit noticeable degradation in discharge capacity compared to the D-LFP dry cathode. At 1.5C rate, the discharge areal capacity of the D-LFP dry cathode remained at approximately 4 mAh cm^{-2}, whereas that of the L-LFP dry cathode dropped to ~3.5 mAh cm^{-2}, likely due to limitations in Li-ion kinetics within the L-LFP dry cathode, stemming from the large particle size of LFP [Figure 5C]. To verify this, EIS was conducted at 50% state of charge (SOC) using a half-cell configuration [Figure 5D][40]. The L-LFP dry cathode exhibited a significantly higher Li-ion resistance of 6.60 Ω, compared to ~4.1 Ω for both D-LFP and S-LFP dry cathodes. Considering the intrinsically low ionic

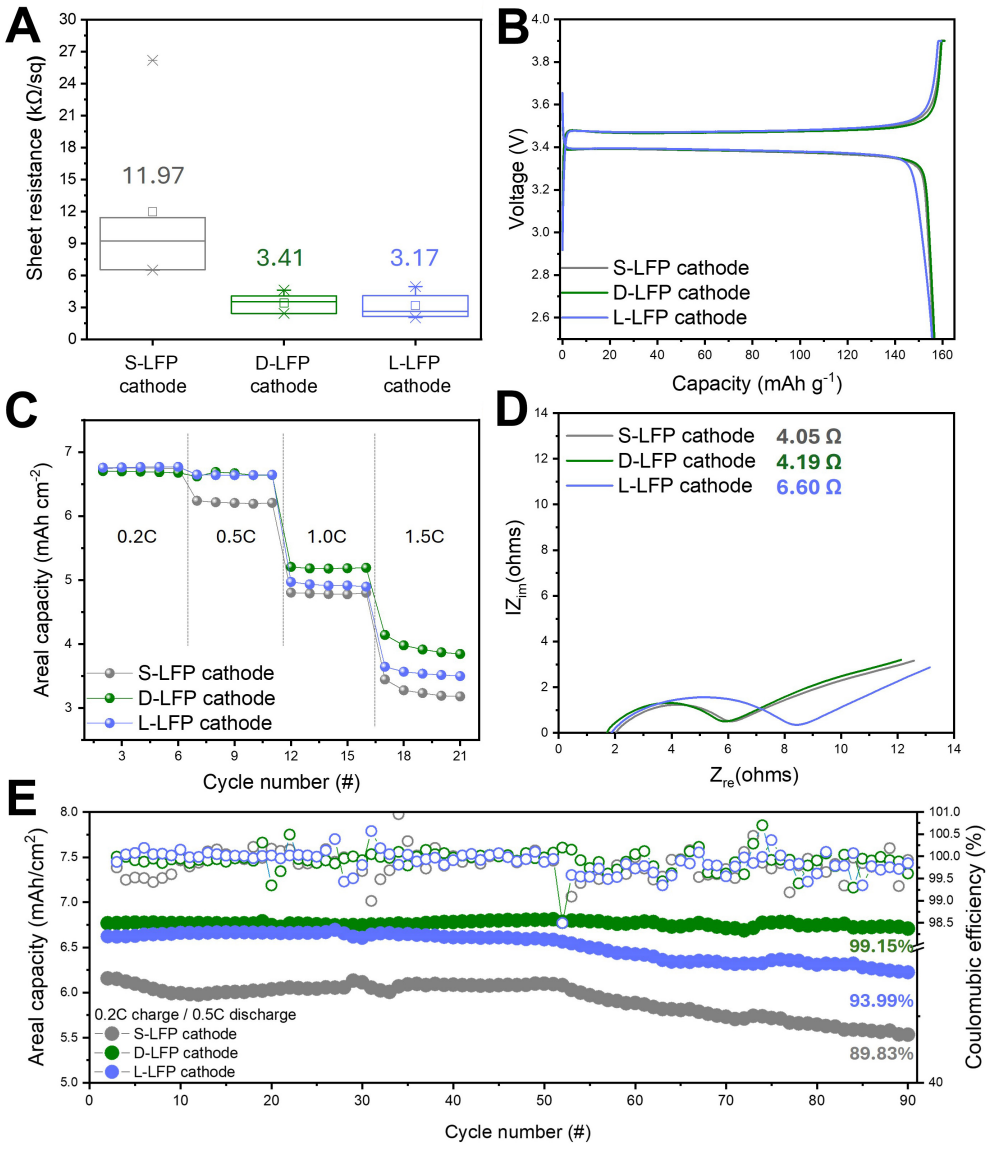


Figure 5. Electrochemical performance of dry LFP cathodes with 7 mAh cm^{-2}. (A) Sheet resistances of dry LFP cathode films; (B) The 1st cycle voltage profiles and (C) rate capability; (D) Li-ion resistance from EIS measurement at SOC 50% and (E) cycle performances at 0.2C-rate charge and 0.5C-rate discharge. LFP: $LiFePO_4$; EIS: electrochemical impedance spectroscopy; SOC: state of charge.

conductivity of LFP, larger particle sizes increase diffusion pathways and reduce Li-ion kinetics, particularly under high current densities, thereby resulting in lower discharge capacities. These results highlight the critical role of particle size of LFP in governing Li-ion kinetics, underscoring the necessity of applying nano-sized LFP to enable high-rate performance. In addition to rate performance, the long-term cycling stability of the electrodes was evaluated. Under 0.2C-rate charge/discharge cycles, all LFP dry cathodes exhibited comparable capacity retention, indicating no significant degradation differences at low current densities [Supplementary Figure 15]. However, at higher discharge rate conditions-0.2C-rate charging followed by 0.5C-rate discharging-the D-LFP cathode demonstrated the most stable capacity retention over extended cycles, clearly outperforming both S-LFP and L-LFP [Figure 5E]. This superior cycling stability is attributed to the low electronic and Li-ion resistances of the D-LFP cathode, as well as its enhanced mechanical integrity, which effectively suppresses particle detachment and maintains continuous electronic pathways during repeated high-rate discharging. Collectively, these results highlight that the two-step extrusion process, by enabling the formation of long and thick PTFE fiber networks within nano-sized LFP

dry cathodes, enhances flexibility and mechanical robustness. This enhanced mechanical integrity preserves both the electrode microstructure and continuous electron pathways, effectively lowering electronic and ionic resistances. Overall, the D-LFP dry cathode offers the most balanced combination of mechanical robustness and electrochemical performance, outperforming both S-LFP and L-LFP in terms of electronic conductivity and Li-ion resistance. These advantages translate into superior rate capability and cycling stability, even under conditions of low binder content and high areal loading of active material.

Nevertheless, despite the significant improvements, the mechanical properties of nano-sized LFP dry cathodes still fall short compared to those of dry cathodes based on high-nickel cathode or graphite anodes. These limitations continue to pose challenges for the application of roll-to-roll dry coating processes. Future research should, therefore, focus on further enhancing the mechanical properties of nano-sized LFP dry cathodes. In particular, materials-level innovations, when combined with advanced process engineering, will be essential to fully unlock the potential of nano-LFP dry cathodes for scalable, high-performance lithium-ion batteries.

CONCLUSION

In this study, we developed a simple yet effective two-step extrusion process to control the distribution and morphology of PTFE fibers within nano-sized LFP dry cathode films, without modifying the material composition. This process-driven approach enabled the formation of a dual-scale PTFE fiber network-comprising both short and thin PTFE fiber network from the 1st stage extrusion and thick and long PTFE fiber network from the 2nd stage extrusion, which significantly enhanced the flexibility and mechanical robustness of nano-sized LFP dry cathode films, even at low binder content (2 wt%). As a result, the nano-sized LFP dry cathode films exhibited improved film-forming capability, reduced electrical resistance, and superior electrochemical performance, including superior rate capability and cycling stability under high areal capacity (7 mAh cm^{-2}). Nevertheless, further enhancement of mechanical properties is still needed for full compatibility with roll-to-roll processes. This could be achieved by integrating materials-level innovations with the developed PTFE fiber network engineering process. Such a synergistic approach would further advance the dry coating process technology for nano-sized LFP dry cathodes and accelerate the scalable production of next-generation, high-performance LFP-based lithium-ion batteries.

DECLARATIONS

Authors' contributions

Conceptualization, writing - original draft: Kim, J.; Kim, M.
Experiments and data collection: Han, S.
Supervision, review and editing: Paik, U.; Song, T.

Availability of data and materials

The datasets supporting the findings of this study are included within the article and its Supplementary Materials files. Further data are available from the corresponding authors upon reasonable request.

Financial support and sponsorship

This work was supported by the Technology Innovation Program (or Industrial Strategic Technology Development Program-Materials & Components Technology Development Program) (20024261, Development of thick film electrode and cell manufacturing technology for high-performance lithium iron phosphate battery with energy density of over 200 Wh/kg) funded By the Ministry of Trade, Industry & Energy (MOTIE, Korea). This work was also supported by the Technology Innovation Program (00429527, Development of high-density thick-film Lithium Manganese Iron Phosphate electrode manufacturing technology through application of functional conductive materials) through the Korea Planning & Evaluation Institute of Industrial Technology (KEIT) funded by the Ministry of Trade, Industry & Energy (MOTIE, Korea). This work was also supported by Samsung SDI.

Conflicts of interest

All authors declared that there are no conflicts of interest.

Ethical approval and consent to participate

Not applicable.

Consent for Publication

Not applicable.

Copyright

© The Author(s) 2026.

Supplementary Materials

Supplementary Materials

REFERENCES

1. Yang, Z.; Huang, H.; Lin, F. Sustainable electric vehicle batteries for a sustainable world: perspectives on battery cathodes, environment, supply chain, manufacturing, life cycle, and policy. *Adv. Energy. Mater.* **2022**, *12*, 2200383. DOI
2. Frith, J. T.; Lacey, M. J.; Ulissi, U. A non-academic perspective on the future of lithium-based batteries. *Nat. Commun.* **2023**, *14*, 420. DOI PubMed PMC
3. Jamil, S.; Wang, G.; Fasehullah, M.; Xu, M. Challenges and prospects of nickel-rich layered oxide cathode material. *J. Alloys. Compd.* **2022**, *909*, 164727. DOI
4. Li, W.; Erickson, E. M.; Manthiram, A. High-nickel layered oxide cathodes for lithium-based automotive batteries. *Nat. Energy.* **2020**, *5*, 26-34. DOI
5. Nekahi, A.; Kumar, M. R. A.; Li, X.; Deng, S.; Zaghib, K. Sustainable $LiFePO_4$ and $LiMn_xFe_{1-x}PO_4$ (x=0.1-1) cathode materials for lithium-ion batteries: a systematic review from mine to chassis. *Mater. Sci. Eng. R. Rep.* **2024**, *159*, 100797. DOI
6. Ramasubramanian, B.; Sundarrajan, S.; Chellappan, V.; Reddy, M. V.; Ramakrishna, S.; Zaghib, K. Recent development in carbon-$LiFePO_4$ cathodes for lithium-ion batteries: a mini review. *Batteries* **2022**, *8*, 133. DOI
7. Zhong, Z.; Chen, L.; Zhu, C.; Ren, W.; Kong, L.; Wan, Y. Nano $LiFePO_4$ coated Ni rich composite as cathode for lithium ion batteries with high thermal ability and excellent cycling performance. *J. Power. Sources.* **2020**, *464*, 228235. DOI
8. Yang, X.; Liu, T.; Wang, C. Thermally modulated lithium iron phosphate batteries for mass-market electric vehicles. *Nat. Energy.* **2021**, *6*, 176-85. DOI
9. Gao, F.; Tang, Z.; Xue, J. Preparation and characterization of nano-particle $LiFePO_4$ and $LiFePO_4$/C by spray-drying and post-annealing method. *Electrochim. Acta.* **2007**, *53*, 1939-44. DOI
10. Ji, G.; Wang, J.; Liang, Z.; et al. Direct regeneration of degraded lithium-ion battery cathodes with a multifunctional organic lithium salt. *Nat. Commun.* **2023**, *14*, 584. DOI PubMed PMC
11. Kuang, Y.; Chen, C.; Kirsch, D.; Hu, L. Thick electrode batteries: principles, opportunities, and challenges. *Adv. Energy. Mater.* **2019**, *9*, 1901457. DOI
12. Wu, J.; Zhang, X.; Ju, Z.; et al. From fundamental understanding to engineering design of high-performance thick electrodes for scalable energy-storage systems. *Adv. Mater.* **2021**, *33*, 2101275. DOI
13. Boyce, A. M.; Cumming, D. J.; Huang, C.; et al. Design of scalable, next-generation thick electrodes: opportunities and challenges. *ACS. Nano.* **2021**, *15*, 18624-32. DOI
14. Chang, J. H.; Pin, M. W.; Kim, I.; et al. Binder migration: frequently observed yet overlooked phenomena in electrode processing for lithium-ion batteries. *J. Energy. Storage.* **2024**, *83*, 110729. DOI
15. Lu, Y.; Zhao, C.; Yuan, H.; Hu, J.; Huang, J.; Zhang, Q. Dry electrode technology, the rising star in solid-state battery industrialization. *Matter* **2022**, *5*, 876-98. DOI
16. Sung, K.; Hwang, I.; Choi, J.; Jung, S.; Yoon, J. Enhanced adhesion in PTFE-based dry electrodes with hydrogen bonding co-binder integration for advanced lithium-ion batteries. *Chem. Eng. J.* **2025**, *511*, 161789. DOI
17. Zhang, K.; Li, D.; Wang, X.; et al. Dry electrode processing technology and binders. *Materials* **2024**, *17*, 2349. DOI PubMed PMC
18. Kim, J.; Park, K.; Kim, M.; et al. 10 mAh cm^{-2} cathode by roll-to-roll process for low cost and high energy density Li-ion batteries. *Adv. Energy. Mater.* **2024**, *14*, 2303455. DOI
19. Horst, M.; Beverborg, F.; Bahlmann, L.; et al. Effect of active material morphology on PTFE-fibrillation, powder characteristics and electrode properties in dry electrode coating processes. *Powder. Technol.* **2025**, *451*, 120451. DOI

20. Wang, X.; Chen, S.; Zhang, K.; et al. A polytetrafluoroethylene-based solvent-free procedure for the manufacturing of lithium-ion batteries. *Materials* **2023**, *16*, 7232. DOI PubMed PMC
21. Lee, K.; Jo, Y.; Nam, J. S.; Yu, H.; Kim, Y. Dry-film technology employing cryo-pulverized polytetrafluoroethylene binder for all-solid-state batteries. *Chem. Eng. J.* **2024**, *487*, 150221. DOI
22. Kang, J.; Eom, H.; Jang, S.; et al. Bollard-anchored binder system for high-loading cathodes fabricated via dry electrode process for Li-ion batteries. *Adv. Mater.* **2025**, *37*, 2416872. DOI
23. Zhang, Y.; Lu, S.; Wang, Z.; Volkov, V.; Lou, F.; Yu, Z. Recent technology development in solvent-free electrode fabrication for lithium-ion batteries. *Renew. Sustain. Energy. Rev.* **2023**, *183*, 113515. DOI
24. Kwon, K.; Kim, J.; Han, S.; et al. Low-resistance $LiFePO_4$ thick film electrode processed with dry electrode technology for high-energy-density lithium-ion batteries. *Small. Sci.* **2024**, *4*, 2300302. DOI
25. Al-Samet, M. A.; Burgaz, E. Improving the lithium-ion diffusion and electrical conductivity of $LiFePO_4$ cathode material by doping magnesium and multi-walled carbon nanotubes. *J. Alloys. Compd.* **2023**, *947*, 169680. DOI
26. Naoi, K.; Kisu, K.; Iwama, E.; et al. Ultrafast charge-discharge characteristics of a nanosized core-shell structured $LiFePO_4$ material for hybrid supercapacitor applications. *Energy. Environ. Sci.* **2016**, *9*, 2143-51. DOI
27. Luo, Y.; Chen, Y.; Koratkar, N.; Liu, W. Densification of alloying anodes for high energy lithium-ion batteries: critical perspective on inter- versus intra-particle porosity. *Adv. Sci.* **2024**, *11*, 2403530. DOI PubMed PMC
28. Wiegmann, E.; Fischer, S.; Leeb, M.; Kwade, A. Sustainable lithium ferro-phosphate cathode manufacturing: a semi-dry approach with water-based processing and polytetrafluoroethylene binders. *Batteries* **2023**, *9*, 567. DOI
29. Kim, B.; Kim, D. K.; Yu, J.; Yoo, Y. Conductive agent-controlled tortuosity in solvent-free thick-film electrodes for high-energy lithium-ion batteries. *Energy. Environ. Mater.* **2025**, e70019. DOI
30. Wang, X. Q.; Chen, D. R.; Han, J. C.; Du, S. Y. Crystallization behavior of polytetrafluoroethylene (PTFE). *J. Appl. Polym. Sci.* **2002**, *83*, 990-6. DOI
31. Starkweather, H. W.; Zoller, P.; Jones, G. A.; Vega, A. J. The heat of fusion of polytetrafluoroethylene. *J. Polym. Sci. Polym. Phys. Ed.* **1982**, *20*, 751-61. DOI
32. Ferry, L.; Vigier, G.; Vassoille, R.; Bessede, J. L. Study of polytetrafluoroethylene crystallization. *Acta. Polym.* **1995**, *46*, 300-6. DOI
33. Jiang, R.; Liu, T.; Xu, Z.; Park, C. B.; Zhao, L. Improving the continuous microcellular extrusion foaming ability with supercritical CO_2 of thermoplastic polyether ester elastomer through in-situ fibrillation of polytetrafluoroethylene. *Polymers* **2019**, *11*, 1983. DOI PubMed PMC
34. Jiang, G.; Hu, Z.; Xiong, J.; Zhu, X.; Yuan, S. Enhanced performance of $LiFePO_4$ originating from the synergistic effect of graphene modification and carbon coating. *J. Alloys. Compd.* **2018**, *767*, 528-37. DOI
35. Kim, I.; Choi, J. H.; Jang, H.; et al. Troubleshooting carbon nanotube bundling using electrostatic energy-driven dispersion for $LiFePO_4$ bimodal thick electrode in lithium-ion batteries. *ACS. Nano.* **2025**, *19*, 15941-52. DOI
36. Launey, M. E.; Ritchie, R. O. On the fracture toughness of advanced materials. *Adv. Mater.* **2009**, *21*, 2103-10. DOI
37. Soderholm, K. J. Review of the fracture toughness approach. *Dent. Mater.* **2010**, *26*, e63-77. DOI PubMed
38. Seidl, C.; Thieme, S.; Frey, M.; Nikolowski, K.; Michaelis, A. Comparison of electronic resistance measurement methods and influencing parameters for LMFP and high-nickel NCM cathodes. *Batteries* **2024**, *10*, 105. DOI
39. Li, H.; Peng, L.; Wu, D.; Wu, J.; Zhu, Y.; Hu, X. Ultrahigh-capacity and fire-resistant $LiFePO_4$-based composite cathodes for advanced lithium-ion batteries. *Adv. Energy. Mater.* **2019**, *9*, 1802930. DOI
40. Zhang, B.; Wang, L.; Zhang, Y.; Wang, X.; Qiao, Y.; Sun, S. G. Reliable impedance analysis of Li-ion battery half-cell by standardization on electrochemical impedance spectroscopy (EIS). *J. Chem. Phys.* **2023**, *158*, 054202. DOI

Disclaimer/Publisher's Note: All statements, opinions, and data contained in this publication are solely those of the individual author(s) and contributor(s) and do not necessarily reflect those of OAE and/or the editor(s). OAE and/or the editor(s) disclaim any responsibility for harm to persons or property resulting from the use of any ideas, methods, instructions, or products mentioned in the content.

© The Author(s) 2026. Open Access This article is licensed under a Creative Commons Attribution 4.0 International License (https://creativecommons.org/licenses/by/4.0/), which permits unrestricted use, sharing, adaptation, distribution and reproduction in any medium or format, for any purpose, even commercially, as long as you give appropriate credit to the original author(s) and the source, provide a link to the Creative Commons license, and indicate if changes were made.